33RD INTERNATIONAL COSMIC RAY CONFERENCE, RIO DE JANEIRO 2013
THE ASTROPARTICLE PHYSICS CONFERENCE

Highlights in Solar and Heliospheric Physics - Rapporteur Report

RAÚL GÓMEZ-HERRERO[1]

[1] *Space Research Group, Department of Physics and Mathematics, University of Alcalá, E-28871, Alcalá de Henares, Spain*

raul.gomezh@uah.es

Abstract: This paper summarizes the works presented during the Solar and Heliospheric (SH) parallel sessions of the 33rd International Cosmic Ray Conference (ICRC) held in Rio de Janeiro, Brazil in July 2013.

Keywords: Galactic Cosmic Rays, Solar Cosmic Rays, Solar Energetic Particles, Cosmic Ray Modulation, Solar Cycle, Solar Flares, Coronal Mass Ejections, Space Weather, Ground Level Enhancements, Forbush Decreases, Instrumentation

1 Introduction

This paper aims to summarize the works presented during the Solar and Heliospheric (SH) parallel sessions of the 33rd International Cosmic Ray Conference (ICRC) held in Rio de Janeiro, Brazil in July 2013. Even though it tries to cover all the the major topics and results presented during the conference, this paper is based in the subjective author's perspective and restricted to space limitations. Only those papers presented during the conference and submitted for publication in the conference proceedings have been considered for this overview. At the time of writing these lines and according to the conference website (`http://www.cbpf.br/~icrc2013/`), 127 (out of a total of 939) contributions were presented during the SH parallel sessions of the ICRC 2013. These contributions were divided in three sections, distributed as follows:

- Experimental results: 71 contributions (29 oral, 42 poster)
- Theory, models and simulations: 34 contributions (15 oral, 19 poster)
- Methods, techniques and instrumentation: 22 contributions (5 oral, 17 poster)

The comparison with the ICRC 2011 (204 SH papers published in proceedings) and with earlier editions of the conference evidences a decrease in the number of SH contributions and in the relative number of SH papers with respect to the total number of contributions. While the SH section is still a significant part of the ICRC ($>$ 13 % of the papers), this tendency raises some concern for future editions.

The paper is organized as follows: In section 2 we discuss the main contributions related to solar cosmic rays (solar energetic particles, ground level enhancements, etc.). Section 3 is devoted to models and observations of non-solar cosmic rays in the heliosphere, including among other topics modulation models and observations for galactic cosmic rays, Forbush decreases and other energetic particle populations such as Jovian electrons. Papers related to instrumentation and data access tools are discussed in section 4.

2 Solar energetic particles

2.1 Multipoint observations of solar energetic particle events

A topic of major interest during the last years, in coincidence with the rising phase of solar cycle 24 and the full-Sun coverage provided by the STEREO mission [1], has been the study of the longitudinal dependences of Solar Energetic Particle (SEP) event properties [2, 5, 6, 10, 7]. Multi-point observations of SEP events combining the twin STEREO and near-Earth spacecraft show that the peak intensity and the total fluence during SEP events decrease with increasing separation angle between the spacecraft magnetic footpoint and the source Active Region (AR). Following earlier studies (e.g. [8]), this angular dependence can be represented by a Gaussian distribution [9, 6]. Some studies found east-west asymmetries in the distribution, slightly broader for sources eastward from the spacecraft footpoint [10] or an eastward shift of the distribution centroid [9], which has been interpreted in terms of shock geometry, flux-tube corotation and interplanetary transport through the Parker topology of the interplanetary magnetic field [9, 10].

The physical mechanisms responsible for the broad azimuthal spread of energetic particles observed during some SEP events remain under debate. Many of the events showing broad angular spreads are accompanied by shock signatures (e.g. [6]). Particle acceleration and injection at broad shock waves driven by Coronal Mass Ejections (CMEs) propagating through the corona and the interplanetary medium provide a suitable explanation for broad particle spreads during large gradual events showing clear association with fast CMEs, shocks and type II radio-bursts. However, STEREO observations have shown that the angular particle spread during impulsive ^{3}He-rich events (where the acceleration is commonly assumed to take place at relatively small source regions) can range from relatively narrow to unexpectedly broad [11, 12]. Interplanetary medium conditions can be disturbed e.g. by the presence of previous CMEs, contributing to this variability. A well studied example of impulsive event showing broad particle spread is the the February 7, 2010 ^{3}He-rich event [12, 11], observed by ACE and the two STEREO spacecraft, covering an angular interval of 136° in longitude. Results from Potential Field Source Surface (PFSS) models suggest that magnetic field line spreading below the solar wind source surface is unlikely the root cause for the broad particle dis-

tribution [12, 11]. Perpendicular diffusion in the interplanetary medium has been often proposed as a suitable mechanism to explain the particle spread, and particle transport simulations including this effect have been successfully used to explain ion and electron observations during both, impulsive [13],[14] and gradual [15] events. Certain observational features such as the long onset time delays for bad connected spacecraft [6] and the "reservoir effect" could be explained in terms of perpendicular diffusion (e.g. [16, 17]). Wang et al. [17] explained the observational features during the March 1, 1979 gradual SEP event observed by IMP8 and the two Helios spacecraft, when IMP8 was not connected to the shock, combining a shock-acceleration scenario and perpendicular diffusion in the interplanetary medium. Values of the perpendicular to parallel mean free path ratio used to explain the observations of multi-spacecraft SEP events strongly vary from event to event, ranging from 0.04 [17] to 0.15 [14] or even larger [15].

Mewaldt et al. [2] presented observations of the July 23, 2012 SEP event which was associated with a >3000 km/s CME and was characterized by extreme SEP intensity. The event was associated with a slow mode shock and was a remarkable example of a "cosmic-ray mediated shock" because SEP and magnetic pressure were comparable in magnitude. The intense flux of energetic particles likely modified the plasma conditions so that the physical processes changed from those of a supersonically driven blast wave to those of a subsonically driven compressional disturbance [4]. Numerical simulations of the acceleration process at cosmic ray modified shocks were presented by [3], which calculated the maximum momentum of the accelerated particles.

A comparison of large "GOES class" SEP events during the early years of cycles 23 and 24 presented by [2], shows that the total proton fluence during the first 4.5 years of cycle 23 was 2.6 times as great as in cycle 24. Therefore, cycle 24 SEP activity appears to be considerably weaker, as are other indices such as sunspot number, flare size, and geomagnetic storm size and frequency.

2.2 ^{3}He-rich events

Bucik et al. [18] presented in-situ observations of ^{3}He-rich events successively observed by STEREO-A and ACE, combined with PFSS models and EUV imaging, showing the existence of long lasting sources of ^{3}He. These regions are the source of "recurring ^{3}He-rich SEP events". Comparison of events from the same source consecutively observed by different spacecraft show no significant temporal variation in the ^{3}He enrichment.

Data from the ULEIS and SIS instruments onboard ACE show that up to now, the ^{3}He presence at 1 AU is significantly less frequent for cycle 24 compared with a similar period during cycle 23 [19] (Figure 1). These data also show that the ^{3}He variation is best correlated with the sunspot number than with other solar activity parameters.

Kecskemety et al. [20] used ACE/ULEIS data to investigate the spectra and relative abundances of suprathermal ^{3}He, ^{4}He, C, O and Fe ions during quiet-time periods in the 23rd and 24th solar cycles. The analysis indicates the presence of different ion acceleration processes during quiet time periods. The comparison of results obtained for the last two solar cycles showed clear differences both in the ion energy spectra and in the energy dependence of relative abundances, probably related to differences in the acceleration conditions in the corona.

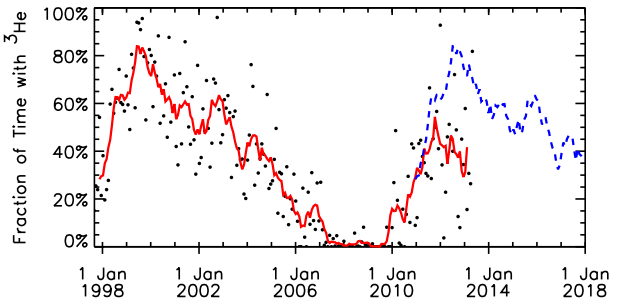

Figure 1: Fraction of the time that ^{3}He from impulsive SEP events was detected by ACE/ULEIS and/or ACE/SIS. Points show values for individual 27-day Bartels rotations. Solid red curve is a 7-rotation smoothing of these values. The dashed blue curve is a copy of the solid red curve shifted to the right so that its rise will approximately match the rise at the start of cycle 24 (from [19]).

2.3 The May 17, 2012 Ground Level Enhancement

The first (an up to now the only) Ground Level Enhancement (GLE) of Solar Cycle 24, attracted considerable attention during the ICRC 2013. This event labeled as GLE71 was Associated with a M5.1 flare on May 17, 2012, starting at 1:25 UT, originating from NOAA A11476 active region located at N11W76. The event was accompanied by a fast halo CME (>1500 km/s) and a type II radio burst, signature of a shock propagating through the corona. The event was observed by different stations of the world-wide neutron monitor network, starting at 01:54 UT at Oulu neutron monitor [21] and by muon telescopes [22]. According to [21], the pitch-angle distribution obtained from multiple neutron monitor data shows a gap at pitch angles 90 and strong anisotropy during the initial phase of the event. After 2:30 UT the anisotropy becomes less evident. The NM64 and "bare" (without lead) neutron monitors at South Pole and the IceTop ice Cherenkov detectors (part of the Ice-Cube Neutrino Observatory) measured the event, with time profiles characterized by a pulse-like enhancement with a peak just after 2:00 UT followed by a broader enhancement (see Figure 2). The yield function of the Polar Bares peaks at lower energy than that of the NM64 tubes and IceTop yield functions peak at still higher energies, therefore the combination of these measurements and the appropriate yield functions provides spectral information. These measurements and the derived primary energy spectrum using were presented by [23]. Preliminary analysis of the IceTop spectrum suggests a major steepening at high energies.

Heber et al. [5] presented multipoint observations of this event, which was detected by both STEREO spacecraft, widely separated from the optimal connection. STEREO-A observed an interplanetary shock followed by an Interplanetary Coronal Mass Ejection (ICME) on May 18. Only the well connected location (Earth) measured strong anisotropies during the early phase of the event. Poor anisotropies and long onset delays at both STEREO suggest that perpendicular interplanetary transport plays a relevant role. A remarkable unexplained feature is that in spite

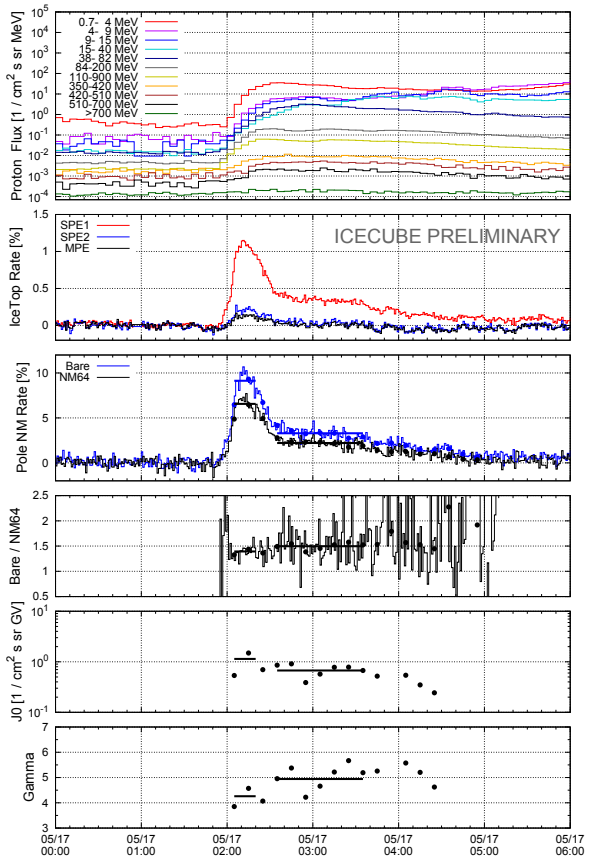

Figure 2: Observations of GLE 71. From top to bottom: GOES-13 proton channels, IceTop rates and South- Pole bare and NM64 neutron monitor rates, ratio of Bare/NM64 monitor, estimated parameters of primary spectrum from Polar Bare analysis as amplitude J0 and exponent γ of a power law in momentum (from [23]).

of the worse magnetic connection, the nearly-relativistic electron onset was observed earlier at STEREO B than at STEREO A.

The PAMELA instrument fills the gap between 100 MeV/n and several GeV/n, providing very valuable for the study of the most energetic SEP events. Bazilevskaya et al [24] presented combined spectra for the GLE 71 and other SEP events using PAMELA, GOES, SOHO/ERNE, neutron monitor and balloon data (Figure 3). The discrepancy between PAMELA and neutron monitor measurements during the early phase of GLE 71 is explained by the strong anisotropy of the first arriving solar protons. Both instruments reach excellent agreement during later phases of the event. PAMELA measured protons up to 1 GeV and He nuclei up to 1.5 GeV/n [25]. Velocity dispersion analysis combining PAMELA, Wind and neutron monitor observations, yields an effective propagation pathlength of 1.64 ± 0.04 AU and a solar release time of 1:41 UT, meaning that the ions were released when the CME height was at 3.9 solar radii [25]. While this delay supports a shock acceleration scenario, the results of velocity dispersion analysis technique should we taken with care (e.g. [26, 27, 28]) and the issue of shock versus flare acceleration contributions during SEP events remains controversial. According to the shock-acceleration model for SEPs presented by [29], the most efficient acceleration of high

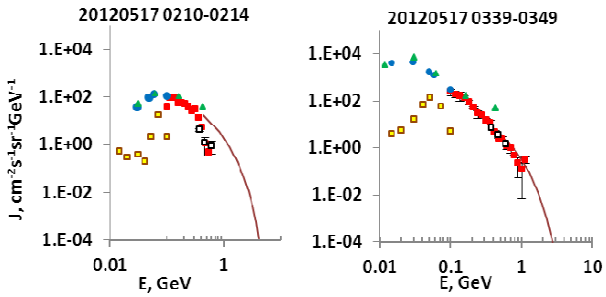

Figure 3: Background-subtracted proton spectra measured during two different time intervals of GLE 71 (time given in format YYYYMMDD HHMM UT). Data from different instruments are combined: red squares - PAMELA, blue circles - GOES 13 EPEAD cpflux, green triangles - GOES 13 EPEAD p17ew, light squares - GOES 13 HEPAD, yellow squares - ERNE HED, brown line - neutron monitor network, brown rhombs - balloon data (from [24]).

energy particles takes place when the shock is below 4 solar radii due to the highest level of Alfvén turbulence and large Alfvénic Mach number, and the highest energy particles are produced around 2 solar radii, being able to accelerate particles up to a maximum energy of 10 GeV for a CME speed of 2500 km/s.

2.4 SEP anisotropies

Leske et al, [30] presented several cases of peculiar 1.8-12 MeV proton anisotropies measured by the Low Energy Telescope (LET) onboard STEREO, including a loss cone distribution during July 24, 2012 (showing a pronounced deficit of particles at pitch-angle 180°), and a trapped distribution (peaking at pitch-angle 90°) starting on May 5, 2013. SEP Pitch-angle distributions are extremely valuable for the study of particle transport (rigidity/velocity dependence of pitch-angle diffusion coefficient), to trace magnetic topology during particle propagation (loss-cone distributions, trapped distributions, etc.) or to identify new particle injections overlapping with previous events (i.e., during multiple solar eruptions [31]) which are not evident in the intensity versus time profiles.

2.5 Solar Neutrons

Solar neutrons carry clean information on the ion acceleration process which cannot be provided by gamma, or energetic proton measurements.The SEDA-FIB (Space Environment Data Acquisition using the FIBer detector) instrument began collecting data at the International Space Station (ISS) in August 2009. It can determine both the energy and arrival direction of solar neutrons. SEDA-FIB observed for the first time solar neutrons likely originated from M-class solar flares that occurred on March 7, June 7, September 24 and November 3 of 2011 and January 23 of 2012 [32]. The X17.0 East-limb solar flare of September 07, 2005 released high-energy neutrons that were detected by the Solar Neutron Telescope at Sierra Negra, Mexico [33]. The neutrons detected had at least 1 GeV energy and the inferred spectral index which best fits the neutron flux is around 3, in agreement with previous works. As the neutrons are essentially unaltered during the interplan-

etary propagation, the resulting spectrum corresponds well to the source spectrum.

2.6 The A.D. 775 event

Miyake et al. [34] studied measurements of ^{14}C content in Japanese tree rings from A.D. 550 to 1100 with 1 to 2-year resolution, and they found two rapid ^{14}C increases corresponding to A.D. 775 and A.D. 993 (see also [35, 36]). These increases are very unlikely explained by supernova explosions because there is no historical observational record of a supernova during that period nor a consistent supernova remnant. A short Gamma Ray Burst (GRB) is also an unlikely explanation because the estimated rate of occurrence of short GRBs is too low (one event in $3.75 \cdot 10^6$ years) to produce two events (A.D. 775 and A.D. 993) in a relatively small time interval. The authors concluded that these increases are most probably related to extreme SEP events. A superflare is also the most likely explanation of the A.D. 775 according to [37]. The same work postulates that a large comet colliding with the sun could produce shock-accelerated GeV cosmic rays in the solar corona and/or solar wind, and possibly account for extreme SEP events like the A.D. 775 event (see also [38]). A comparable event in the modern era could have devastating consequences for power grids and satellite electronics.

3 Non-solar Cosmic Rays in the heliosphere

3.1 Cosmic Ray modulation: observations and transport models

The PAMELA (Payload for Antimatter Matter Exploration and Light Nuclei Astrophysics) instrument [41] has provided multiple measurements of Cosmic Rays at 1 AU during the last solar minimum, which are highly valuable for modulation studies. This experiment is onboard the Resurs DK1 satellite launched in 2006, and comprises a time-of-flight system, a silicon micro-strip magnetic spectrometer, an electromagnetic calorimeter, an anticoincidence system, a shower tail catcher scintillator and a neutron detector [42]. Due to its complex design, PAMELA requires sophisticated data reduction techniques (background elimination, efficiency correction, incident energy reconstruction, etc.). The temporal evolution of proton and helium spectra measured by PAMELA during 2006-2009 were presented by [42] and a preliminary electron and positron measurements during the same period were presented by [43]. Several authors have recently reported that high rigidity cosmic rays reached record intensities during the last solar minimum (e.g. [39, 40]). The highest modulated spectra between 100 MeV and 50 GeV of galactic protons (and other cosmic rays) were recorded by PAMELA in late 2009 [44] (Figure 4). During previous $A < 0$ polarity cycles, proton spectra were always lower than for $A > 0$ cycles at energies below few-GeV, as expected from drift models. The reason is that during $A > 0$ cycles it is easier for low energy positive particles to enter the inner heliosphere mainly through the polar regions of the heliosphere than in an $A < 0$ cycles when they enter mainly through the equatorial region. This is evident when comparing $A > 0$ and $A < 0$ periods with the same activity level, after removing the time lag between sunspot number and the cosmic ray variation at 1 AU [45]. Galactic proton intensities are relative insensitive to changing values of the tilt angle of the heliospheric current sheet during $A > 0$ intervals, while proton intensities

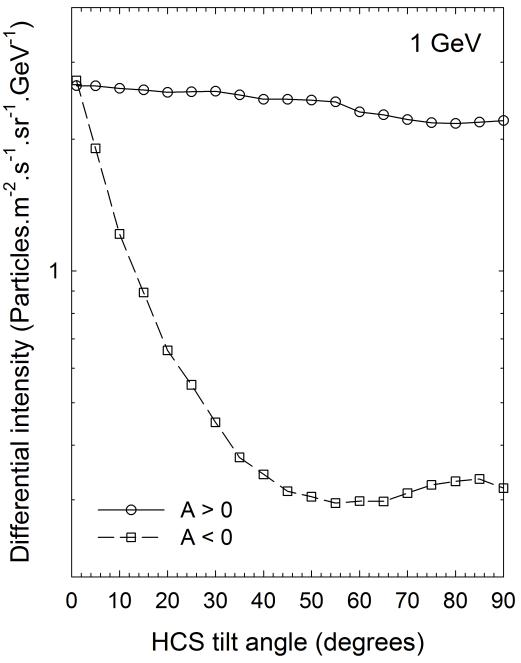

Figure 5: Response of the proton differential intensity at Earth (at E = 1 GeV) to changing values of the tilt angle of the heliospheric current sheet for positive and negative polarity cycles, under the assumption of ideal drifts (from [46]).

strongly decrease with increasing tilt angle for $A < 0$ periods. For very large values of the tilt angle, cosmic rays do not effectively follow the HCS (due to diffusion) and the intensity becomes independent of the tilt angle [46] (Figure 5).

The observations during the last solar minimum described above, suggest that the modulation during the last declining solar activity and solar minimum period (2006-2009) was unusual and clearly different from previous $A < 0$ polarity minima. Solar modulation models indicate that at the same level of solar activity, the proton spectrum for the next solar minimum could be higher than in 2009 and may therefore set a new record [44, 47]. Up to now the sunspot area during solar cycle 24 is much lower than during recent solar cycles, comparable to the Glaisberg minimum in the first decades of the last century (but still much greater than in the Maunder and even Dalton minima), while the galactic cosmic ray intensity is slightly higher than in previous solar cycles [48] (see also [49, 50]). According to [50], the weak cosmic ray modulation during the current 24th solar cycle is connected to several anomalies which have arisen on the Sun and in a heliosphere during recent years, in particular the weakening of solar magnetic fields.

Krainev et al. [51] used a simple modulation model to study the time and energy behavior of the galactic cosmic ray intensity during the last three solar activity minima. They separated the contributions of the main processes contributing to the modulation (drifts, diffusion, convection and adiabatic losses) and studied how they are influenced by changes in different heliospheric parameters. According to their model, the additional flux of low energy par-

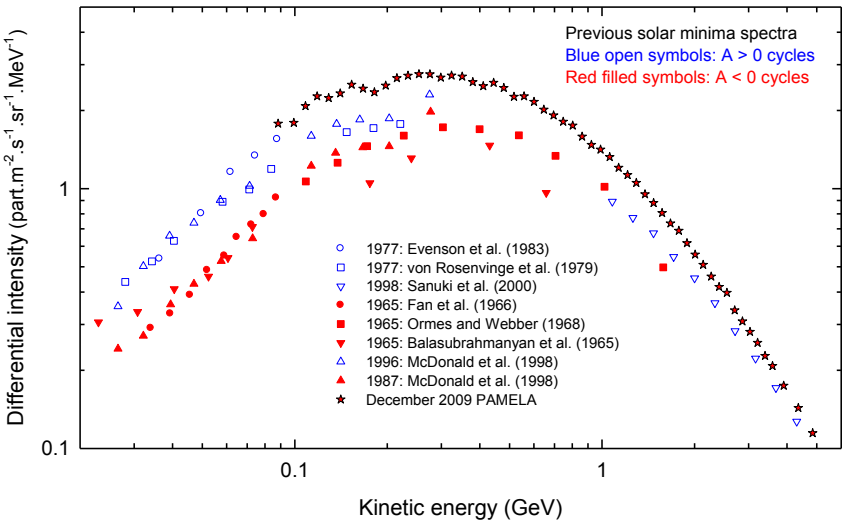

Figure 4: Cosmic Ray proton spectra observed during solar minimum modulation periods of 1965, 1976-77, 1987, 1996-97 and 2009. Note that the spectra for all previous A $>$ 0 cycles (in blue) are consistently higher than for the $A < 0$ cycles (in red) at energies below a few GeV, except for the 2009 spectrum (from [44]).

ticles in 2009 with respect to 1987 is due mainly to enhanced diffusion rather than drift. The 2D time-dependent modulation model presented by [52] is in good agreement with observations at 1 AU (IMP 8) and along Voyager 1 and Ulysses trajectories, over multiple solar cycles (1985-2009). This model includes time-dependence in the diffusion and drift coefficients. The analysis of the temporal variations during the recent solar minimum using this model suggests that solar-cycle-related changes in diffusion coefficients (due to the changes in magnetic field magnitude and variance) are more important than the changes in the drift coefficient (due to the tilt angle variations). The model failed to reproduce step-like increases or decreases in the cosmic ray intensities during solar maximum, indicating that the variations of magnetic field measured at 1 AU cannot be simply transported to the outer heliosphere, but a more realistic scenario including merging of the propagating barriers in the form of global interaction regions is required in order to reproduce such observations.

According to [53], the analysis of neutron monitor, space and balloon-borne cosmic ray measurements, suggests that after 1980 an energy dependence of the modulation of lower energy galactic cosmic rays became evident, with softer energy spectrum at minima of solar activity. The spectrum became steeper in each subsequent minimum for solar cycles 21/22, 22/23, and 23/24 and no such behavior was observed at higher energy. Kalinin et al. [47] used a simple modulation model to study the unusually soft cosmic ray spectrum during the last solar minimum (see also [51]). They were able to reproduce the main observational features of the galactic cosmic rays during the solar minima between cycles 21/22 and 22/23 assuming an effective size of the modulation region with $r_{max} = 125$ AU and an exponent for the rigidity dependence of the diffusion coefficients $R = 1$. In order to reproduce the unusually soft energy dependence for the last minimum (2009), the size of the modulation region needs to be reduced to $r_{max} = 90$AU and the rigidity dependence index to $R = 0.9$. Alania et al. [54] investigated the relationship between the cosmic ray intensity changes dI and the magnitude of the interplanetary magnetic field B during 1996-2012. They found an inverse lineal correlation between them, which becomes weaker close to the solar maximum. The dependence of dI on B can be represented by a power law, $dI \propto B^{\alpha}$.

The steady state 3D modulation model for protons presented by [55] was used to study the unusually quiet recent $A < 0$ solar minimum. Temporal variations of the tilt angle of the heliospheric current sheet and the heliospheric magnetic field magnitude alone are not sufficient to explain the observations and temporal variations of the diffusion coefficients are required. The analysis suggests that the proton mean free paths had to increase (the turbulence had to weaken) with time below ~ 3 GeV in order to reproduce the high fluxes observed by PAMELA. Both, diffusion and drifts had a comparable contribution to the observed intensity increase at 1 GeV from November 2006 to December 2009 and there is a complicated interplay of all these effects. The diffusion effect dominates in the low energy part. Similar analysis was presented for electrons by [56], showing that in spite of the exceptional conditions during the last solar minimum, drift effects and charge-sign-dependent modulation becomes evident when comparing electrons and protons (Figure 6). As found for protons below 3 GeV, the electron mean free paths below 500 MV were required to increase from 2006 onward in order to reach observed intensities at the end of 2009. The importance of drift effects in charge-dependent modulation was also highlighted by [57], which compared out-of ecliptic Ulysses observations and simulation results from the two-dimensional HelMod Montecarlo simulation model.

Strauss et al. [58] presented a new hybrid model to study galactic cosmic ray modulation. It combines a three-dimensional magneto-hydrodynamic model to define the heliosphere and a stochastic differential equation cosmic ray transport model. The authors used this model to investigate the modulation along the Voyager 1 trajectory, using different scenarios for the radial dependence of the parallel mean free path. They concluded that modulation continues beyond the Heliopause and predicted that Voyager 1 should continue measuring a small positive radial gradient.

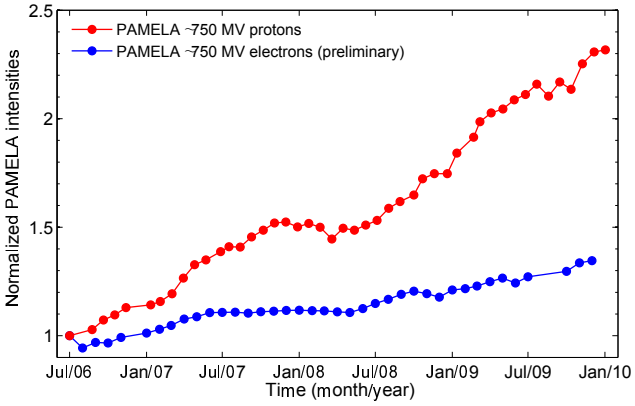

Figure 6: PAMELA $\sim$ 750 MV protons and preliminary electrons normalized to July 2006, as a function of time, illustrating the charge-sign dependent modulation (from [56]).

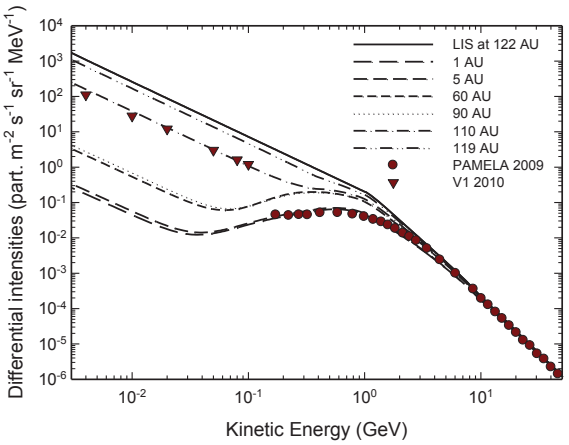

Figure 7: Computed modulated electron spectra at Earth and different heliocentric locations (from 5 to 119 AU and polar angle 60°, corresponding to the Voyager 1 trajectory), compared with observations from Voyager 1 (2010) and from PAMELA (2009). The heliopause spectrum (upper solid line) is specified at the heliopause, positioned in the model at 122 AU (from [60]).

Changes of the parallel mean free path values inside the heliopause affect the modulation beyond the heliopause (due to cosmic ray mobility across the heliopause), therefore solar cycle effects may have measurable effects in this region. Changing only the parallel mean free path has almost no effect in the amount of modulation beyond the heliopause, which according to the model results, is described mainly by the parallel-to-perpendicular mean free path ratio. This result is explained due to the fact that cosmic rays have to diffuse perpendicular to interstellar magnetic field lines in order to penetrate the heliosphere.

A heliopause spectrum for cosmic ray electrons at 122 AU, over an energy range from 1 MeV to 50 GeV was presented by [59] and [60]. This spectrum can be considered the lowest possible limit for the Local Interstellar Spectrum (LIS) and was obtained combining a 3D energy-dependent numerical modulation model, Voyager 1 observations of 6-120 MeV electrons in the outer heliosphere and PAMELA observations of >200 MeV electrons at 1 AU. This LIS has a double power law form in energy, with exponent -1.55 for energies below 1 GeV and -3.15 for energies above 5 GeV. This steeper spectrum at high energies is required to reproduce the electron spectrum observed by PAMELA in 2009 (Figure 7). The spectral break between 0.8 and 2 GeV is consistent with previous results [61]. The model reproduces the large amount of modulation of galactic electrons below 100 MeV in the inner heliosheath. At low energies the Jovian electrons are the dominant contribution to the electron spectrum observed inside 20 AU. At 12 MeV, the upper limit for galactic electrons at 1 AU is $2.5 \cdot 10^{-1}$ electrons/(m^2 s sr MeV) [59] (Figure 8).

3.2 Jovian Electrons

As mentioned above, in absence of SEP events, Jupiter is a dominant source of electrons observed in the near-Earth space around 10 MeV. These electrons show a 13-month periodicity corresponding to the synodic period of Jupiter. Superposed to this periodicity, Co-rotating Interaction Regions (CIR) cause flux depressions (27-day variations). Modeling efforts can reproduce the basic observational features of these periodicities [62]. Apart from the orbital motion of Jupiter with respect to the Earth, varying solar wind speed defines the fraction of Earths orbit where direct connection with Jupiter is possible along the interplanetary magnetic field lines [63]. The observation of Jovian electrons during periods when this connection is not possible suggest a relevant role of perpendicular diffusion in the interplanetary medium. An alternative explanation is that Jovian electrons could be confined inside magnetic traps co-rotating with the Sun, and reach the Earth or STEREO during bad connection periods [64]. A preliminary electron spectra observed by SOHO/EPHIN between 0.2-5.0 MeV can be approximated by a double power-law with a break around 0.5 MeV [63].

3.3 Forbush decreases

Several papers studied the magnitude of Forbush Decreases (FDs) as a function of the cosmic ray rigidity. Kojima et al. [68] used data from 17 different neutron monitor stations and the large area multidirectional muon telescope of GRAPES-3 at Ooty, India, to study the extent of FDs at different rigidities (rigidity spectrum) for 26 FDs during 2000-2011. The average primary rigidity dependence shows a double power-law behavior with exponent -0.65 for the neutron monitor stations (rigidity interval 10-32 GV) and -1.26 for the muon telescope (64-92 GV). Kravtcova and Sdovnov [69] studied the cosmic ray rigidity spectrum and anisotropy during a FD in March 2012. The spectrum from 7 to 50 GV during different time intervals can be reproduced by a power law in rigidity with exponents varying from -0.86 to -1.00. Ahluwalia et al. [70] obtained the hourly rigidity spectrum for a FD observed in May 2005 using data from neutron monitors and multidirectional muon telescopes. This FD was caused by a halo CME observed on May 13, 2005 and extended to rigidities $\leq$200 GV. The timelines for neutron monitors show that the FD onset happened shortly after a storm sudden commencement, while the onset observed at higher rigidities by muon telescopes was delayed by $\sim$5 hours. The calculated rigidity spectrum has an exponent -1.05, in agreement with the force field theory. The evolution of the exponent studied with hourly resolution shows a value -1 near the minimum of FD which becomes softer during the recov-

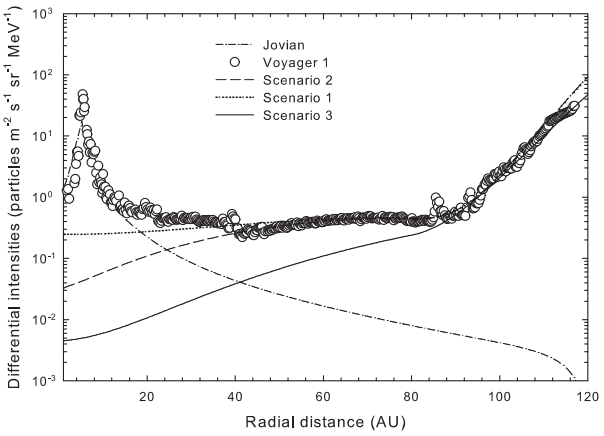

Figure 8: Computed radial dependence of 12 MeV galactic electrons shown for three scenarios, together with Voyager 1 observations (6-14 MeV) of galactic and Jovian electrons since 1977. This radial profile is dominated by Jovian electrons up to 20 AU, depending on which scenario is picked, whereas galactic electrons dominate clearly from r $>$ 80 AU (from [59]).

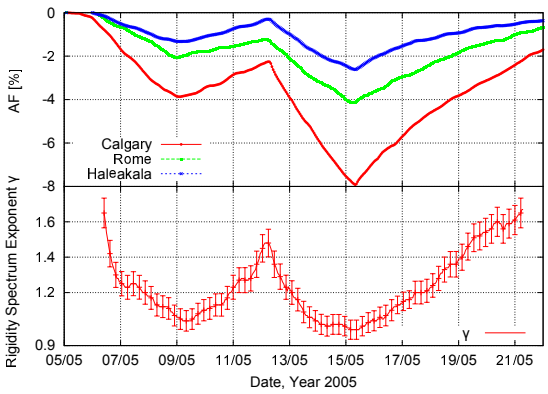

Figure 9: Timelines of the cosmic ray intensity smoothed over 73 hours (upper panel) for Calgary, Rome and Haleakala neutron monitors and the power-law exponent of the rigidity spectrum during the 5-25 May 2005 Forbush decrease. (from [70])

ery phase (Figure 9). The authors attributed the changes of the exponent to changes in the interplanetary magnetic field turbulence. This relationship was found during several FDs and is expected due to the rigidity-dependence of the the parallel diffusion coefficient ($\kappa \propto R^{2-\nu}$), where ν is the exponent of the power spectral density of the interplanetary magnetic field ([71] and references therein).

A number of papers studied FD observations from a Space Weather perspective. For instance, [72] analyzed magnetic cloud properties, geoeffectiveness and cosmic ray muon decreases during 2009-2011. The percentage of Magnetic Clouds (MCs) followed by intense or moderate geomagnetic storms (geoeffectiveness) is 52.9%, much lower than previous cycles. They concluded that MCs that drive fast shocks are more geoeffective and cause larger cosmic ray muon decreases. Parnahaj et al. [73] presented a statistical study of the relation between the amplitude of FDs, the associated geomagnetic activity and different characteristics of the associated CMEs and ICMEs. They found a clearer correlation between FD amplitude and CME speed and acceleration for those events associated with halo CMEs. Cosmic ray anisotropy detected using global neutron monitor data [74] or directional muon telescope data [75] show changes several hours before the arrival of interplanetary disturbances and the subsequent geomagnetic storm, which provides a valuable signature for space weather forecasting (see also [76]). Muon detectors with directional capabilities provide muon anisotropy data during heliospheric disturbances, which yield unique information about the structure and dynamics of these events [75].

Kryakunova et al. [77] studied the recurrent cosmic ray decreases caused by high speed streams originating from coronal holes during 2007. This period was ideal for the study of this kind of decrease because solar activity was very low and there was only a limited number of CME-related FDs. They found that the magnitude of the decreases was correlated with the interplanetary magnetic field parameters (magnitude and critical cosmic ray rigidity) but not with the solar wind speed.

The BESS-Polar I balloon-borne experiment [78] allows precise identification of cosmic ray helium isotopes, providing for the first time measurements of isotopic fluxes. BESS-Polar I measurements during December 13-21, 2004 show that the fluxes of cosmic protons, ^{3}He and ^{4}He in the 1.2-2.5 GV rigidity ranges varied similarly during this period (probably coincident with the recovery of a decrease caused by a magnetic cloud or a co-rotating interaction region [79]). The time variations are more pronounced than those observed at higher rigidities by the CLIMAX neutron monitor, consistent with changes of solar activity that should affect low-rigidity particles more strongly.

3.4 27-day variations and other cosmic ray periodicities

Gil and Alania [80] investigated the temporal behavior of the galactic cosmic ray intensity, solar wind parameters, sunspot number and other heliospheric observational data measured at 1 AU during 2009-2013. Using harmonic analysis, they found a quasi-periodicity of three to four Carrington rotation period. They proposed that this recurrence is related to a similar cycle on the topological structure of the solar magnetic field and is consequence of the combination of the turbulent solar dynamo and the differential rotation of the sun. A study of the harmonics of the 27-day variations of the galactic cosmic rays, solar wind velocity and interplanetary magnetic field during the last solar minimum (2007-2009) was presented by [81]. The quasi-periodic changes found, show the existence of a stable a 26-27 day periodicity. Similar changes were observed for the cosmic ray intensity during 2007-2008, but during 2009 the cosmic ray intensity showed a gradual increase of the period up to 33-36 days. The authors attributed this change to the influence of high-latitude changes at the Sun in coincidence with the onset of the new cycle. The solar wind and magnetic field observations are insensitive to these changes because they reflect only changes in source regions located near the solar equator, while cosmic rays are affected by global changes in the 3-D heliosphere. Wawrzynczak and Alania [71] studied the temporal variation of the galactic cosmic ray intensity from June 14 to September 13, 1994. This period is dominated by the

second harmonic of the 27-day variations (∼14 day periodicity). These variations are likely correlated with similar periodic changes in the interplanetary magnetic field turbulence levels.

Gil and Alania [82] presented a 3-D theoretical model of the 27-day variations of the galactic cosmic ray intensity in connection with solar wind parameters for different epochs of the solar activity cycle. The variations of the in situ measurements of solar wind speed and magnetic field magnitude included in the model can explain the observational result. The rigidity spectrum of the 27-day cosmic ray variation is hard (power law exponent -0.8) near the solar maximum and softer (-1.3) at solar minimum. The same authors studied the temporal variations of the rigidity spectrum exponent for the period 1970-2004 and found periodicities of 142.9 $\pm$ 1.6 and 35.7 $\pm$ 1.7 Carrington rotations (10.6 and 2.6 years, respectively). Shorter periodicities of 26.6 $\pm$ 1.2 and 14.5 $\pm$ 0.7 Carrington rotations (2.0 and 1.1 years, respectively) are found when considering only the data period 1976-1982.

Laurenza et al. [83] studied the tilt angle of the heliospheric current sheet (which characterizes the drift effects on CRs) using the empirical mode decomposition technique. They found a 5-6 year periodicity in the cosmic ray intensity and the tilt angle which is not present in the sunspot area. They suggested that this tilt-angle periodicity is responsible for the peaked-flat maximum feature observed in the cosmic ray intensity during odd-even numbered cycles.

3.5 Long term cosmic ray anisotropies

Munakata et al [84] analyzed the long-term variations of the three-dimensional anisotropy of galactic cosmic rays during the period 1971-2011, observed by neutron monitors (covering ∼10 GV primary cosmic rays) and the Nagoya muon detector (responding to ∼50 GV primary cosmic rays). The free-space harmonic vector of the diurnal anisotropy clearly shows a phase shift from 18 h local solar time during $A < 0$ intervals to earlier hours during $A > 0$ solar minima. This shifting is more prominent at high rigidities (muon data). The anisotropy component perpendicular to the magnetic field is significantly larger for the muon data (high rigidity) than for neutron monitors (low rigidity), while the parallel anisotropy components are comparable for both datasets. This rigidity dependence of the perpendicular anisotropy is likely the origin of the larger phase shift observed in the muon diurnal anisotropy. The same authors found a clear correlation of the magnitude of the parallel anisotropy with the solar wind velocity. The radial density gradient anticorrelates with the parallel mean free path (derived from the values of the anisotropy), with systematic higher values of the radial gradient during $A < 0$ periods. These result were confirmed by [85] (Figure 10, who analyzed the long-term variation (1992-2012) of the first order anisotropy provided by the Global Muon Detector Network (GMDN) on hourly basis.

3.6 Cosmic ray shadow of the Sun

Observations of high-energy cosmic rays at TeV energies using detectors with directional capabilities such as the ARGO-YBJ experiment in Tibet [86] and the Tibet air shower array [87] found that the distribution of arrival directions show a deficit corresponding to the location of the Sun. This deficit in the cosmic ray flux caused by the Sun acting as an obstacle is called cosmic ray "shadow"

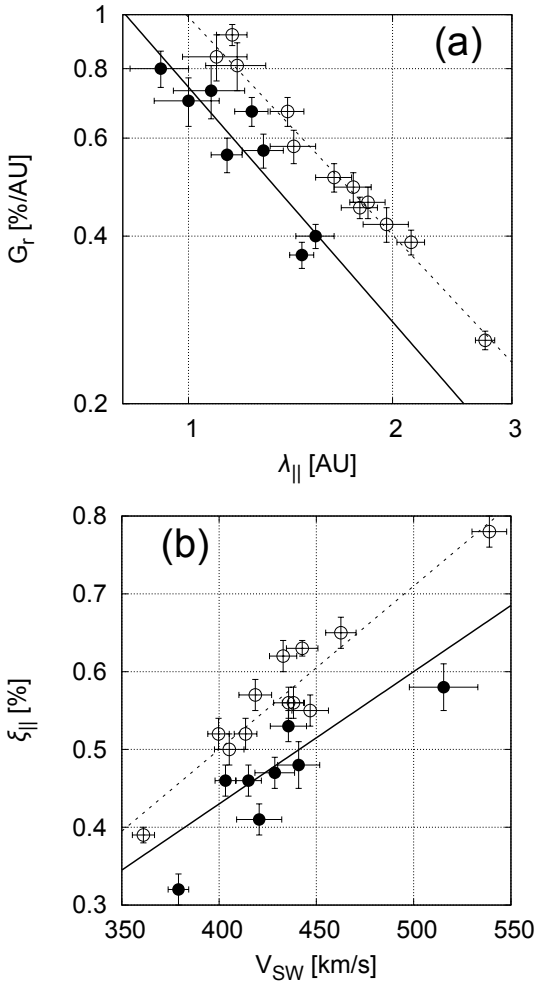

Figure 10: Results derived from muon anisotropy data: (a) Scatter plot between the parallel mean free path $\lambda_{||}$ and the radial gradient G_r. (b) Scatter plot between the solar wind speed V_{SW} and the parallel anisotropy $\xi_{||}$. In each panel, the solid circles with the solid regression line represent the yearly mean values in $A > 0$ solar polarity epoch (1992-1999) while the open circles with the dotted regression line represent yearly mean values in $A < 0$ (2001-2012) (from [85]).

and is slightly shifted from the location of the solar disk in the sky due to the deflection in the cosmic ray trajectory caused by the solar, interplanetary and Earth's magnetic fields. ARGO-YBJ measurements during the period 2008-2012 provided a continuous monitoring of the cosmic ray shadow of the Sun on a quarterly-basis. The authors concluded that the shadow appears clearly at the beginning of 2008 and progressively becomes less evident as the solar maximum approaches. They found a clear anticorrelation between the cosmic ray deficit and the sunspot number and solar radio-flux at 10.7 cm. The anticorrelation between the cosmic ray shadow and the solar activity levels was also found by [87], who studied the evolution of the cosmic ray shadow for the period 2000-2009 using the Tiber air shower array (Figure 11). They concluded that the shadow reaches a maximum size at the solar minimum (2009) and almost disappears near the solar maximum (2000), when the solar magnetic fields are stronger and have more complexity. Montecarlo simulations of the

cosmic particle propagation in the coronal magnetic field using PFSS models are in progress and can help to understand the relation between the solar magnetic field variations and the strength, shape and shifting of the cosmic ray shadow.

3.7 Thunderstorm-related particles

During recent years several observational studies have linked energetic particle detection at ground level and thundercloud and/or a lightnings (e.g. [88] and references therein). Measurements of the atmospheric electric field and observations of the Tibet Air Shower Array [89] registered since February 2010 show evidences of energetic particle increases with the passage of thunderclouds. [90] presented observations of thermal neutron variations measured at ground by unshielded scintillation neutron detectors. They studied the variations of the amplitude of Forbush decreases as a function of different absorber thickness above the detector, obtaining a clear anti-correlation which could be potentially useful for neutron spectroscopy studies. The same paper pointed out the importance of taking precautions against electromagnetic noise when studying neutron variations during thunderstorms, the authors studied the counting rates during thunderstorms and no evidences of the "thunderstorm neutrons" effect were found during two summer periods of data recorded.

4 Instrumentation and data access tools

New ground-based experiments were presented during the ICRC 2013, some of them are primarily intended for high-energy cosmic ray studies but provide capabilities for Solar and Heliospheric Science and Space Weather studies. The HAWC (High Altitude Water Cherenkov Array) instrument being installed at Sierra Negra, Mexico, 4100 m above sea level, consists of 300 large cylindrical water Cherenkov detectors covering an area of 22000 m^2. It will start operating at the end of 2013. Although its primary goal is the detection of high energy gammas, it will also be sensitive to solar events (GLEs, Forbush decreases, solar neutrons and solar gamma rays), offering high energy, time and angular resolution. Forbush decreases detected by the HAWC-VAMOS engineering array and by the HAWC-30 array (HAWC first step, with 30 water Cherenkov detectors) in March 2012 [91] and in April 2013 [92] were presented and compared with neutron monitor data. Observations of the March 2012 Forbush decrease by the LAGO (Large Aperture Gamma ray bursts Observatory) experiment were presented by [93]. LAGO is a network of water Cherenkov detectors (WCDs) located in different Latin American countries. The experiment is designed for the detection of the highest energy component of GRBs but can be used to study the solar modulation of galactic cosmic rays and other transient effects. The SciCRT (SciBar for the Cosmic Ray Telescope) project [65, 66, 67] is a solar neutron and cosmic ray muon hodoscope that will soon start measurements at Sierra Negra (Mexico), 4600 m above sea level. The instrument consists of 14848 scintillator bars. A wavelength shifting fiber is inserted in each scintillator bar and the scintillation signals are detected by multi anode photo multiplier tube. Coincidence of the top and bottom layers are used as muon trigger, while neutrons do not trigger the anticoincidence and are identified by recoil protons produced inside the detector. SciCRT will offer high angular resolution and four times more sensitivity to solar neutrons than current Solar Neutron Telescopes such as SONTEL, operating in Sierra Negra since 2003 [95]. A new concept of relatively inexpensive and portable mini neutron monitors was presented by [96]. These units are manufactured as already-calibrated units that are not dismantled in transport which may affect their efficiencies. Due to the extreme increase in the price of the ^{3}He isotope, these units as well as other new neutron monitor stations (e.g. [97]) have reverted to the $^{10}BF_3$ counter tubes instead of using ^{3}He tubes.

Orlando and Strong [98] presented the StellarICs (Stellar and solar Inverse Compton emission) software package for calculating the gamma-ray emission from Inverse-Compton (IC) scattering by cosmic-ray leptons in the heliosphere and in the photospheres of stars (and the Sun). It includes a set of cosmic-ray spectra and a formulation of their modulation, but it can be used for any user-defined modulation model and lepton spectra. The software is used in the Fermi-LAT Science Tools as a standard model for the solar IC emission. It is publicly available, stays under continuous development and it will be especially useful for evaluating Fermi-LAT data.

Labrador et al. [99] presented an indirect method developed by Sollit et al. [100] for estimating mean ionic charge states for SEP events from energy-dependent decay timescales derived from the exponential decays of SEP intensities. This indirect method could provide very important information on e.g. the longitudinal dependence of charge states during SEP events observed from multiple locations, however the initial analysis of a sample of STEREO and ACE SEP events shows that the method can be only applied for a limited number of cases.

SEPServer [101] is a collaborative project to provide access to state-of-the-art observations and analysis tools for the scientific community on SEP events. A SEP event catalog based on Ulysses observations from 1996 to the end of the mission was presented by [101]. Different characteristics of these events were determined and compared with simulation-based analysis and remote sensing observations. The catalog will be available to the community for further analysis through `http://server.sepserver.eu`.

The Standard Radiation Environment Monitors (SREMs) flying on several European Space Agency (ESA) missions provide the largest amount of space radiation data for ESA [102]. A database providing electron, proton and cosmic ray data for six SREMs units from 2002 until now and a repository providing documentation, response matrices and analysis software are available for registered users.

Several papers used data from the Global Muon Detector Network (GMDN) [72, 103, 104, 105, 106] and the Neutron monitor database (NMDB) [74, 77, 107, 108, 21, 109]. These instrument networks are providing cosmic ray measurements at ground level, very useful for the study of Forbush decreases, cosmic ray modulation and GLEs. The NMDB is now providing neutron monitor data to the scientific community with open data access (`http://www.nmdb.eu/`) on a routine basis and with increasing geographic coverage (e.g. [97]) resulting in a wide data visibility which boosts scientific productivity of neutron monitor data.

Buetikofer et al. [110] presented a critical review of the reliability of GLE analysis based on neutron monitor data. The authors concluded that the GLE characteristics for an individual GLE published in the literature by different

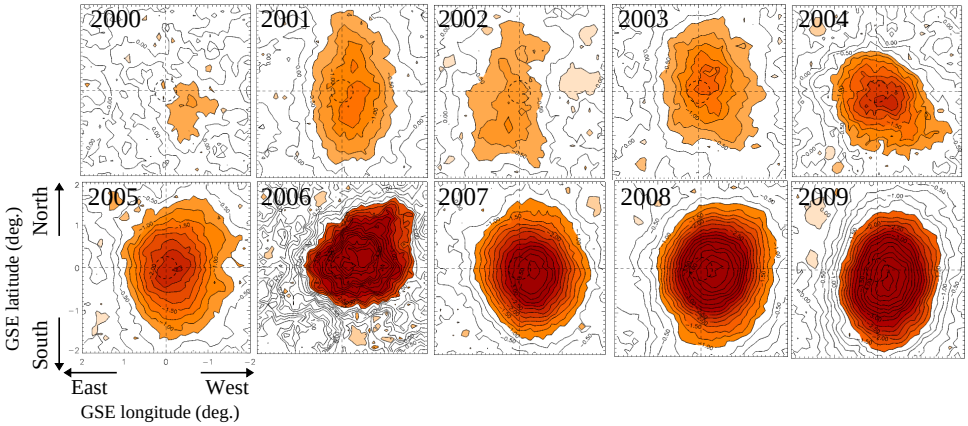

Figure 11: Yearly variation of the cosmic ray shadow of the Sun observed at 3 TeV from 2000 to 2009. Each panel shows the two-dimensional contour map of the cosmic-ray flux deficit in the GSE coordinates (from [87]).

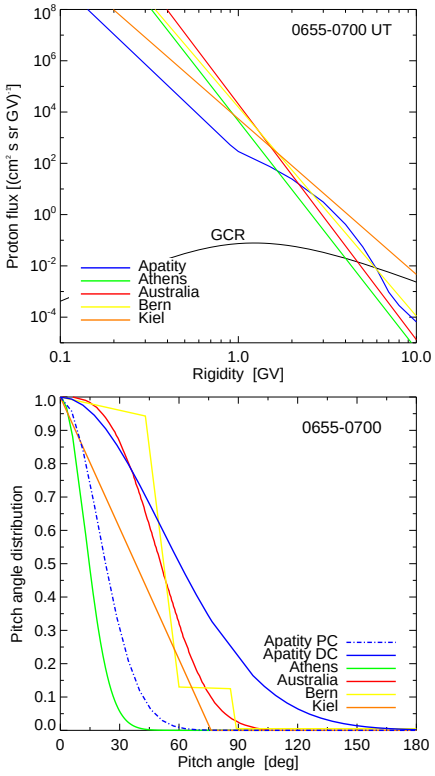

Figure 12: Solar cosmic ray spectra (top) and pitch angle distributions (bottom) during the main phase of GLE69 as derived from neutron monitor data by different groups.

groups can show important discrepancies, raising a word of caution in the validity of quantitative results (see Figure 12). These differences are present even for stations using the same yield function and their origin has not been yet identified. A more detailed exchange of information on the different GLE analysis procedures used by different groups is highly recommended.

As mentioned in previous sections, space-based instrumentation (STEREO, Voyager, PAMELA, ACE and SOHO among others) are an essential contribution for the study of cosmic rays in the heliosphere, particularly in the low energy part of the spectrum not accessible for ground-based instruments. Indirect measurements of cosmic rays can be derived from instruments not initially intended for particle detection. Oh et al. [111] presented a technique to quantify the number of cosmic ray traces registered by SOHO/EIT imaging data. This method provides an estimation of the cosmic ray flux and permits the identification of Forbush decreases, SEP events and the long term cosmic ray variations with the solar activity cycle. Upcoming missions currently in preparation such as Solar Orbiter and Solar Probe Plus intend to revolutionize our understanding of the particle acceleration processes at the Sun and in the heliosphere. The Integrated Science Investigation of the Sun (ISIS) experiment onboard the upcoming Solar Probe Plus mission, planned for launch in 2018, which will approach to 10 solar radii of the Sun was presented by [112]. The instruments part of ISIS will cover the energy range from 0.02 to >100 MeV/nucleon for all the major ion species and 0.03 to 3 MeV for electrons, being also able to detect energetic neutral atoms, neutrons and gammas. These measurements will enable the study of the the seed populations, acceleration and particle transport processes in the heliosphere.

5 Summary and Conclusions

The last solar minimum between solar cycles 23 and 24 showed very low levels of solar activity and the highest cosmic ray intensities recorded at 1 AU since the space age. The highest modulated proton spectrum between 100 MeV and 50 GeV was recorded at the end of 2009. These observations suggest that the modulation during the last solar minimum was unusual compared with previous $A < 0$ polarity minima and is being intensively studied using sophisticated modulation models combined with observations in the inner and outer heliosphere. The study of the different contributions to the modulation is complicated due to the interplay between different processes, but enhanced diffusion due to temporal changes in the diffusion coefficient (meaning a turbulence weakening) could have played a major role in this cosmic ray enhancement. Measurements from the exceptional location of Voyager 1, with its recently confirmed crossing of the heliopause [113], combined with models and observations at 1 AU provide unique insights for the study of the modulation processes.

The new cycle (now reaching the maximum), has also shown considerable weaker activity up to now, compared

with previous cycles. This is evidenced by different parameters such as the sunspot area, the geomagnetic activity levels, the total fluence of 10 MeV protons or the fraction of time with suprathermal ^{3}He in the interplanetary medium. The STEREO mission combined with the complete fleet of near-Earth spatial observatories and ground based instruments has provided unprecedented in-situ and remote-sensing observations of SEP events from multiple points at 1 AU. Particularly important are those events where widely separated spacecraft observed energetic particles originating from the same active region. The role played in the angular particle spread by different physical processes such as shock acceleration, coronal transport in diverging magnetic field lines or cross-field diffusion in the interplanetary medium remains under study. In spite of the low activity, strong SEP events such as the July 23 event have been observed from space, however only one GLE (the GLE 71 on May 17, 2012) has been detected up till now by neutron monitors during cycle 24. The GLE 71 has been extensively studied using ground-based and space-based instruments, providing a complete spectral coverage from the very low energies up to the GeV range, as well as directional and timing information. Some theoretical studies suggest that shocks could be able to accelerate particles up to GeV energies, but the long-standing debate about the role of flares and CME-driven shocks for SEP acceleration remains open. Velocity dispersion and timing information at 1 AU should be taken with care due to the effect of particle scattering during the interplanetary propagation (among other effects). Combination of remote-sensing observations at different wavelenghts (including hard X-rays and gamma rays), energetic particles and solar neutrons are very helpful to complete our understanding of the acceleration processes. The study of the ^{14}C content in tree rings has revealed transient increases that support the occurrence of extreme SEP events in the past (e.g. the A.D. 775 event), with intensities well above the observed during the most intense events of the space era. These events would produce serious consequences from the point of view of Space Weather.

The study of the anisotropies and the rigidity dependence during GLEs and Forbush decreases greatly benefits form a world-wide network of neutron monitors and muon telescopes continuously providing data. Measurements of precursor signals in the cosmic ray anisotropies before the arrival of interplanetary disturbances causing Forbush decreases have important an application in short-term Space Weather forecasting. Ground based instruments mostly oriented to the study of high-energy cosmic rays are providing valuable information for solar and heliospheric studies such as the connections between solar activity and the characteristics of the cosmic ray shadow of the Sun or new measurements of Forbush decreases with Cherenkov detectors. Considerable effort is being done to provide cosmic ray data to the scientific community through different projects under open-access policies, contributing to an increase in the scientific outcome of the data.

Acknowledgment:I am grateful to the organizers of the 33rd ICRC in Rio de Janeiro, Brazil for the invitation to give a rapporteur talk and for the financial support to attend the conference. I also acknowledge the financial support from the Spanish Ministerio de Ciencia e Innovación under project AYA2011-29727-C02-01. I am thankful to J.J. Blanco for his help reviewing the manuscript. I apologize for those papers omitted or covered with incomplete level of detail in this report.

References

[1] M. L. Kaiser et al., Space Science Reviews, 136(1-4): 5-16 (2008).
[2] R.A. Mewaldt et al., Proc. 33rd Internat. Cosmic Ray Conf. (Rio de Janeiro) (2013) paper 1186.
[3] X. Wang, N. Wang and Y. Yan Proc. 33rd Internat. Cosmic Ray Conf. (Rio de Janeiro) (2013) paper 0718.
[4] C.T. Russell et al., Astrophysical Journal, 770:38 (2013) 1-5, doi:10.1088/0004-637X/770/1/38.
[5] B. Heber Proc. 33rd Internat. Cosmic Ray Conf. (Rio de Janeiro) (2013) paper 0746.
[6] N. Dresing et al., Proc. 33rd Internat. Cosmic Ray Conf. (Rio de Janeiro) (2013) paper 0611.
[7] S. V. Tasenko et al., Proc. 33rd Internat. Cosmic Ray Conf. (Rio de Janeiro) (2013) paper 0616.
[8] D. Lario et al., Astrophysical Journal 653 (2006) 1531.
[9] D. Lario et al., Astrophysical Journal 767:41 (2013) 1-17 doi:10.1088/0004-637X/767/1/41.
[10] H. He and W. Wan, Proc. 33rd Internat. Cosmic Ray Conf. (Rio de Janeiro) (2013) paper 0267.
[11] C.M.S. Cohen et al., Proc. 33rd Internat. Cosmic Ray Conf. (Rio de Janeiro) (2013) paper 0802.
[12] M. Wiedenbeck et al. Astrophysical Journal, 762:54 (2013) 1-9 doi:10.1088/0004-637X/762/1/54.
[13] J. Giacalone and J. R. Jokipii, Astrophysical Journal Letters, 751:L33 (2012) 1-5 doi:10.1088/2041-8205/751/2/L33.
[14] G. Qin et al., Proc. 33rd Internat. Cosmic Ray Conf. (Rio de Janeiro) (2013) paper 0174.
[15] N. Dresing et al., Solar Physics 281 (2012) 281-300 doi:10.1007/s11207-012-0049-y.
[16] A. Struminsky, Proc. 33rd Internat. Cosmic Ray Conf. (Rio de Janeiro) (2013) paper 0192.
[17] Y. Wang et al., Proc. 33rd Internat. Cosmic Ray Conf. (Rio de Janeiro) (2013) paper 0041.
[18] R. Bučík et al., Proc. 33rd Internat. Cosmic Ray Conf. (Rio de Janeiro) (2013) paper 0552.
[19] M. E. Wiedenbeck and G.M. Mason, Proc. 33rd Internat. Cosmic Ray Conf. (Rio de Janeiro) (2013) paper 0971.
[20] K. Kecskemety, M.A. Zeldovich and Y.I. Logachev, Proc. 33rd Internat. Cosmic Ray Conf. (Rio de Janeiro) (2013) paper 0197.
[21] Y.V. Balabin et al., Proc. 33rd Internat. Cosmic Ray Conf. (Rio de Janeiro) (2013) paper 0021.
[22] C.R.A. Augusto et al., Proc. 33rd Internat. Cosmic Ray Conf. (Rio de Janeiro) (2013) paper 1121.
[23] The IceCube Collaboration, Proc. 33rd Internat. Cosmic Ray Conf. (Rio de Janeiro) (2013) paper 0368.
[24] G.A. Bazilevskaya et al., Proc. 33rd Internat. Cosmic Ray Conf. (Rio de Janeiro) (2013) paper 0332.
[25] R. Carbone et al., Proc. 33rd Internat. Cosmic Ray Conf. (Rio de Janeiro) (2013) paper 0845.
[26] J. Lintunen and R. Vainio, Astronomy and Astrophysics 420 (2004) 343-350 doi:10.1051/0004-6361:20034247
[27] A. Sáiz et al. Astrophysical Journal 626 (2005) 1131-1137 doi:10.1086/430293
[28] S. Kahler and B. R. Ragot Astrophysical Journal 646 (2006) 634-641 doi:10.1086/504674
[29] E.G. Berezhko, S.N. Taneev, T.YU. Grigor'ev, Proc. 33rd Internat. Cosmic Ray Conf. (Rio de Janeiro) (2013) paper 0078.
[30] R.A. Leske et al., Proc. 33rd Internat. Cosmic Ray Conf. (Rio de Janeiro) (2013) paper 0583.
[31] A. Al-Sawad et al., Proc. 33rd Internat. Cosmic Ray Conf. (Rio de Janeiro) (2013) paper 0490.
[32] Y. Muraki et al., Proc. 33rd Internat. Cosmic Ray Conf. (Rio de Janeiro) (2013) paper 0065.
[33] L.X. González et al., Proc. 33rd Internat. Cosmic Ray Conf. (Rio de Janeiro) (2013) paper 0637.
[34] F. Miyake, K. Masuda, T. Nakamura, Proc. 33rd Internat. Cosmic Ray Conf. (Rio de Janeiro) (2013) paper 0424.
[35] F. Miyake et al., Nature 486 (2012) 240-242.
[36] F. Miyake, K. Masuda and T. Nakamura, Nature Commun. (2013), DOI: 10.1038/ncomms2783.
[37] D. Eichler, Proc. 33rd Internat. Cosmic Ray Conf. (Rio de Janeiro) (2013) paper 0014.
[38] D. Eichler and D. Mordecai, Astrophusical Journal Letters 761(2) (2012) L27 doi:10.1088/2041-8205/761/2/L27.

[39] B. Heber et al., Astrophysical Journal 699 (2009) 1956-1963.
[40] R.A. Mewaldt, et al., Astrophysical Journal Letters 273 (2010) L1-L6.
[41] P. Picozza, et al., Astroparticle Physics, 27(4) (2007) 296-315. doi:10.1016/j.astropartphys.2006.12.002.
[42] V. Di Felice et al. Proc. 33rd Internat. Cosmic Ray Conf. (Rio de Janeiro) (2013) paper 0219.
[43] R. Munini et al. Proc. 33rd Internat. Cosmic Ray Conf. (Rio de Janeiro) (2013) paper 0337.
[44] M.S. Potgieter et al. Proc. 33rd Internat. Cosmic Ray Conf. (Rio de Janeiro) (2013) paper 0119.
[45] Y. Stozhkov et al. Proc. 33rd Internat. Cosmic Ray Conf. (Rio de Janeiro) (2013) paper 0094.
[46] R. D. Strauss and M.S. Potgieter Proc. 33rd Internat. Cosmic Ray Conf. (Rio de Janeiro) (2013) paper 0155.
[47] M.S. Kalinin et al. Proc. 33rd Internat. Cosmic Ray Conf. (Rio de Janeiro) (2013) paper 0297.
[48] M.B. Krainev and M.S. Kalinin Proc. 33rd Internat. Cosmic Ray Conf. (Rio de Janeiro) (2013) paper 0317.
[49] H.S. Ahluwalia and R.C. Ygbuhay Proc. 33rd Internat. Cosmic Ray Conf. (Rio de Janeiro) (2013) paper 0005.
[50] R. Gushchina et al. Proc. 33rd Internat. Cosmic Ray Conf. (Rio de Janeiro) (2013) paper 00157.
[51] M.B. Krainev et al. Proc. 33rd Internat. Cosmic Ray Conf. (Rio de Janeiro) (2013) paper 0305.
[52] S.E.S. Ferreira, R. Manuel and M.S. Potgieter Proc. 33rd Internat. Cosmic Ray Conf. (Rio de Janeiro) (2013) paper 0085.
[53] G.A. Bazilevskaya et al. Proc. 33rd Internat. Cosmic Ray Conf. (Rio de Janeiro) (2013) paper 0274.
[54] M.V. Alania et al. Proc. 33rd Internat. Cosmic Ray Conf. (Rio de Janeiro) (2013) paper 0795.
[55] E.E. Vos et al. Proc. 33rd Internat. Cosmic Ray Conf. (Rio de Janeiro) (2013) paper 0273.
[56] E.E. Vos et al. Proc. 33rd Internat. Cosmic Ray Conf. (Rio de Janeiro) (2013) paper 0276.
[57] P. Bobik et al. Proc. 33rd Internat. Cosmic Ray Conf. (Rio de Janeiro) (2013) paper 1100.
[58] R. D. Strauss et al. Proc. 33rd Internat. Cosmic Ray Conf. (Rio de Janeiro) (2013) paper 0154.
[59] R.R. Nndanganeni and M.S. Potgieter Proc. 33rd Internat. Cosmic Ray Conf. (Rio de Janeiro) (2013) paper 0033.
[60] M.S. Potgieter et al. Proc. 33rd Internat. Cosmic Ray Conf. (Rio de Janeiro) (2013) paper 0070.
[61] A. W. Strong, E. Orlando and T.R. Jaffe, Astronomy and Astrophysics, 534 (2011) A54:1-13.
[62] A. Vogt et al. Proc. 33rd Internat. Cosmic Ray Conf. (Rio de Janeiro) (2013) paper 0908.
[63] P. Kühl Proc. 33rd Internat. Cosmic Ray Conf. (Rio de Janeiro) (2013) paper 0072.
[64] K. Kecskemety Proc. 33rd Internat. Cosmic Ray Conf. (Rio de Janeiro) (2013) paper 0327.
[65] Y. Nagai et al. Proc. 33rd Internat. Cosmic Ray Conf. (Rio de Janeiro) (2013) paper 0392.
[66] Y. Nagai et al.Proc. 33rd Internat. Cosmic Ray Conf. (Rio de Janeiro) (2013) paper 0400.
[67] Y. Munakata et al. Proc. 33rd Internat. Cosmic Ray Conf. (Rio de Janeiro) (2013) paper 0140.
[68] H. Kojima et al. Proc. 33rd Internat. Cosmic Ray Conf. (Rio de Janeiro) (2013) paper 0654.
[69] M.V. Kravtcova and V.E. Sdovnov Proc. 33rd Internat. Cosmic Ray Conf. (Rio de Janeiro) (2013) paper 0008.
[70] H.S. Ahluwalia et al. Proc. 33rd Internat. Cosmic Ray Conf. (Rio de Janeiro) (2013) paper 0798.
[71] A. Wawrzynczak and M.V. Alania Proc. 33rd Internat. Cosmic Ray Conf. (Rio de Janeiro) (2013) paper 0.
[72] E. Echer et al. Proc. 33rd Internat. Cosmic Ray Conf. (Rio de Janeiro) (2013) paper 0037.
[73] I. Parnahaj et al. Proc. 33rd Internat. Cosmic Ray Conf. (Rio de Janeiro) (2013) paper 909.
[74] S.A. Starodubtsev et al. Proc. 33rd Internat. Cosmic Ray Conf. (Rio de Janeiro) (2013) paper 0032.
[75] I.I. Yashin et al. Proc. 33rd Internat. Cosmic Ray Conf. (Rio de Janeiro) (2013) paper 0723.
[76] I.S. Pethukov, S.I. Pethukov and V.G. Grigoriev Proc. 33rd Internat. Cosmic Ray Conf. (Rio de Janeiro) (2013) paper 0399.
[77] O. Kryakunova et al. Proc. 33rd Internat. Cosmic Ray Conf. (Rio de Janeiro) (2013) paper 0835.
[78] N. Picot-Clémente et al. Proc. 33rd Internat. Cosmic Ray Conf. (Rio de Janeiro) (2013) paper 1136.
[79] N. Thakur et al. Proc. 33rd Internat. Cosmic Ray Conf. (Rio de Janeiro) (2013) paper 1088.
[80] A. Gil and M.V. Alania Proc. 33rd Internat. Cosmic Ray Conf. (Rio de Janeiro) (2013) paper 0481.
[81] R. Modzelewska and M.V. Alania Proc. 33rd Internat. Cosmic Ray Conf. (Rio de Janeiro) (2013) paper 0477.
[82] A. Gil and M.V. Alania Proc. 33rd Internat. Cosmic Ray Conf. (Rio de Janeiro) (2013) paper 0479.
[83] M. Laurenza et al. Proc. 33rd Internat. Cosmic Ray Conf. (Rio de Janeiro) (2013) paper 0483.
[84] K. Munakata et al. Proc. 33rd Internat. Cosmic Ray Conf. (Rio de Janeiro) (2013) paper 0039.
[85] M. Kozai et al. Proc. 33rd Internat. Cosmic Ray Conf. (Rio de Janeiro) (2013) paper 0183.
[86] Z. Fengrong for the ARGO-YBJ collaboration Proc. 33rd Internat. Cosmic Ray Conf. (Rio de Janeiro) (2013) paper 0589.
[87] M. Amenomori et al. Proc. 33rd Internat. Cosmic Ray Conf. (Rio de Janeiro) (2013) paper 0340.
[88] F. De Sao Sabbas Tavares Proc. 33rd Internat. Cosmic Ray Conf. (Rio de Janeiro) (2013) paper 1223.
[89] M. Amenomori et al. Proc. 33rd Internat. Cosmic Ray Conf. (Rio de Janeiro) (2013) paper 0505.
[90] V. Alekseenko et al. Proc. 33rd Internat. Cosmic Ray Conf. (Rio de Janeiro) (2013) paper 0568.
[91] M. Castillo et al. Proc. 33rd Internat. Cosmic Ray Conf. (Rio de Janeiro) (2013) paper 0816.
[92] A. Lara for the HAWC collaboration Proc. 33rd Internat. Cosmic Ray Conf. (Rio de Janeiro) (2013) paper 0929.
[93] H. Asorey for the LAGO Collaboration Proc. 33rd Internat. Cosmic Ray Conf. (Rio de Janeiro) (2013) paper 1109.
[94] K. Munakata et al. Proc. 33rd Internat. Cosmic Ray Conf. (Rio de Janeiro) (2013) paper 0039.
[95] Y. Muraki et al. Proc. 33rd Internat. Cosmic Ray Conf. (Rio de Janeiro) (2013) paper 0066.
[96] H. Kruüger, H. Moraal and G.J.J. Benadé Proc. 33rd Internat. Cosmic Ray Conf. (Rio de Janeiro) (2013) paper 1062.
[97] J.J. Blanco et al. Proc. 33rd Internat. Cosmic Ray Conf. (Rio de Janeiro) (2013) paper 0191.
[98] E. Orlando and A.W. Strong Proc. 33rd Internat. Cosmic Ray Conf. (Rio de Janeiro) (2013) paper 0967.
[99] A.W. Labrador et al. Proc. 33rd Internat. Cosmic Ray Conf. (Rio de Janeiro) (2013) paper 1188.
[100] L.S. Sollitt et al., Astrophysical Journal 679 (2008) 910-919 doi:10.1086/587121.
[101] B. Heber et al. Proc. 33rd Internat. Cosmic Ray Conf. (Rio de Janeiro) (2013) paper 0761.
[102] W. Hajdas et al. Proc. 33rd Internat. Cosmic Ray Conf. (Rio de Janeiro) (2013) paper 1224.
[103] R.R.S. De Mendoca et al. Proc. 33rd Internat. Cosmic Ray Conf. (Rio de Janeiro) (2013) paper 0385.
[104] A. Dal Lago et al. Proc. 33rd Internat. Cosmic Ray Conf. (Rio de Janeiro) (2013) paper 1194.
[105] M. Rockenbach et al. Proc. 33rd Internat. Cosmic Ray Conf. (Rio de Janeiro) (2013) paper 0170.
[106] C.R. Braga et al. Proc. 33rd Internat. Cosmic Ray Conf. (Rio de Janeiro) (2013) paper 0386.
[107] V.S. Makhmutov et al. Proc. 33rd Internat. Cosmic Ray Conf. (Rio de Janeiro) (2013) paper 0833.
[108] A. Abunin et al. Proc. 33rd Internat. Cosmic Ray Conf. (Rio de Janeiro) (2013) paper 0198.
[109] H.S. Ahluwalia, M.V. Alania and R. Modzelewska Proc. 33rd Internat. Cosmic Ray Conf. (Rio de Janeiro) (2013) paper 0487.
[110] R. Bütikofer et al. Proc. 33rd Internat. Cosmic Ray Conf. (Rio de Janeiro) (2013) paper 0863.
[111] S. Oh et al. Proc. 33rd Internat. Cosmic Ray Conf. (Rio de Janeiro) (2013) paper 0046.
[112] M.I. Desai et al. Proc. 33rd Internat. Cosmic Ray Conf. (Rio de Janeiro) (2013) paper 0895.
[113] D.A. Gurnett et al., Science 341 6153 (2013) 1489-1492, DOI: 10.1126/science.1241681.